Biocatalysis and Agricultural Biotechnology 22 (2019) 101398

Contents lists available at ScienceDirect

Biocatalysis and Agricultural Biotechnology

journal homepage: http://www.elsevier.com/locate/bab

Synergistic and antagonistic effects in simultaneous adsorption of Pb(II) and Cd(II) from aqueous solutions onto chitosan functionalized EDTA-silane/mGO

Afsaneh Shahbazi *, Niloufar Nekouei Marnani, Zeinab Salahshoor

Environmental Science Research Institute, Shahid Beheshti University, Tehran, 1983969411, Iran

ARTICLE INFO

Keywords:
Simultaneous adsorption
Binary solution
Lead
Cadmium
Nano-composite

ABSTRACT

In the present work, EDTA-sinale as a chelating and claw-like substance grafted onto magnetic graphene oxide (mGO). The EDTA/mGO was subsequently functionalized by chitosan as a natural material with glucosamine backbone containing a high density of amino groups. The obtained nano-bio-composite was successfully characterized, and the magnetic field assisted adsorption was used for adsorption of Pb(II) and Cd(II) in single and binary solution in batch system. The optimum pH of 5 and sorbent dosage of 0.3 g/L were obtained in the single-component adsorption for both studied ions. According to single-component adsorption, the maximum adsorption capacity of the CS/EDTA-silane/mGO was achieved to be 2.33 and 1.05 mmoL/g for Pb(II) and Cd(II), respectively, at optimum condition of pH and sorbent dosage. The adsorption kinetic models followed the pseudo-first order kinetic model ($k_{1,Pb(II)} = 0.2145\ min^{-1}$ and $k_{1,Cd(II)} = 0.0815\ min^{-1}$). Thermodynamically, the adsorption of both metal ions was spontaneous and endothermic. The experimental data of binary adsorption show that the effect of Cd(II) on Pb(II) adsorption is synergetic exhibiting there is no competition between ions. Whereas, the effect of the co-existence Pd(II) on Cb(II) adsorption onto CS/EDTA-silane/mGO was found to be antagonistic/inhibition at higher molar concentration ratio of Pb(II).

1. Introduction

Discharge effluent from several industries including agriculture, pharmaceutical, metal plating, mining, leather tanning and electronic manufacturing contain various type of heavy metal ions (Soetaredjo et al., 2013; Wang et al., 2017). Although, the amount of heavy metal ions in wastewater of these industries might be not significant, but it can accumulate in plant and animal's bodies. Thus, they become a severe threat for environment and humans' health (Luo et al., 2015; Liu et al., 2018). In addition, even the very low amount of heavy metal ions such as lead and cadmium can be carcinogenic and pernicious for living organism (Li et al., 2015a, b). Hence, removal of these toxic contaminants becomes a major concern. Different kinds of methods including membrane separation, coagulation, flocculation and adsorption have been utilized for removing heavy metal ions from aqueous solutions (Luo et al., 2015). Ease of operation, flexibility, high rate of efficiency and financial feasibility are the major reasons that introduce adsorption method more beneficial among other conventional techniques (Shahbazi and Zonoz, 2015). While several research focused on reporting different kinds of adsorbents which could remove single pollutant from aqueous solution, the number of research on multicomponent adsorption of heavy metal ions is low (Kyzas et al., 2015; Huang et al., 2019). The multicomponent adsorption is challenging process for researchers due to the limited number of available sites on surface of adsorbent and the antagonist interactions between various heavy metal ions in a solution, (Yan et al., 2016; Sellaoui et al., 2018).

Among different carbon-based materials, graphene oxide for its abundant oxygen containing functional groups and unique structure has received increasing attention for removal of heavy metal ions (Li et al., 2015a, b). Having various oxygen containing functional groups including carboxyl, hydroxyl and epoxy could create many available sites on a surface of GO for anchoring heavy metal ions (Madadrang et al., 2012; Saleh and Gupta, 2014). Beside many potential positive features of graphene oxide, separating GO from aqueous solution could be time-consuming process and may cause water pollution. Adding magnetic particles such as Fe_3O_4 on the surface of GO can help to remove adsorbent from aqueous solution rapidly. The ease of recovery by permanent magnet and reusability of adsorbent as well as heavy

* Corresponding author.
E-mail address: a_shahbazi@sbu.ac.ir (A. Shahbazi).

https://doi.org/10.1016/j.bcab.2019.101398
Received 1 July 2019; Received in revised form 16 October 2019; Accepted 19 October 2019
Available online 22 October 2019
1878-8181/

metal ions, become an important environmental and economic merits of this method (Beheshti et al., 2016; Chen et al., 2019).

Functionalizing the surface of mGO with other functional groups can enhance the adsorptive performance of adsorbent for removing heavy metals (Marnani and Shahbazi, 2019). In this study, Ethyl-enediaminetetraacetic acid (EDTA) is chosen to be an EDTA-sinale as a chelating and claw-like substance which is grafted to the surface of mGO with silylation process (Hou et al., 2010; Ren et al., 2014). The chelate structure of EDTA and abundant amine groups make it an ideal candidate to immobilize and adsorb cationic heavy metal ions (Madadrang et al., 2012; Liu et al., 2018). Carpio, mangaldao et al. (2014) were synthesized EDTA-GO which showed very high adsorption capacity for Pb(II) and Cu(II). They approved that the GO–EDTA did not present any cytotoxicity to human corneal epithelial cells.

With growing the use of various types of adsorbent and consequently advent of their disadvantages for environment, the concern of using biodegradable and nontoxic bio materials as an adsorbent increase. Many research reports that chitosan as a low cost and high-efficient bio adsorbent which have expand application and potential in removal of cationic dyes, proteins and heavy metal ions (Padilla-Ortega et al., 2013; Wang et al., 2016). Chitosan has enormous economic value because of its flexible biological properties. Indeed, its biocompatibility, antioxidant, anticancer, biodegradability, antimicrobial, and non-toxic properties as well as being an economical material, produced from waste resources such as seafood shells make chitosan so favorable for environmental usage. Also, the glucosamine backbone of chitosan contains a high density of functional groups including amine (-NH_2) and hydroxyl (-OH) groups on surface of a chitosan which generate electro-interaction and several unoccupied sites to capture cationic heavy metal ions makes CS as reliable adsorption enhancer (Soetaredjo et al., 2013; Wang et al., 2016; Chen et al., 2019).

In this study, after synthesizing and functionalizing GO by Fe_3O_4 magnetic nanoparticles, EDTA-silane was anchored to the mGO surface by covalence band. Then chitosan bio-polymer was cross-linked to the surface of EDTA-silane/mGO and made environment friendly nano-bio composite for adsorption of Pb(II) and Cd(II). For understanding the adsorption behavior, not only the kinetic, thermodynamic, and isotherm studies were done in single-component, but also the type of metal ion competition was studied in the binary solution with various molar ration concentration of Pb(II) and Cd(II). In addition, three famous multi-component isotherm models were fitted to the binary isotherm data.

2. Materials and methods

2.1. Chemicals

EDTA-silane (N-trimethoxysilylpropyl) -ethyl-enediamine triacetate trisodium salt and the medium molecular weight chitosan powder with 190–310 kDa were purchased from Chemlab (zedelgem, Belgium). Glutaraldehyde 25%, acid acetic and ammonia solution 25% were supplied from Merck (Germany). The Hydrogen peroxide (H_2O_2) 30%, Potassium persulfate ($K_2S_2O_8$) and Sulfuric acid (H_2SO_4) 98% were obtained from Chemlab (zedelgem, Belgium). The stock standard solutions of metals (abbreviated as Cd(II) and Pb(II)) were prepared from Sigma-Aldrich (Germany).

2.2. Preparation of nano-bio composite

2.2.1. Synthesis of magnetic graphene oxide

The graphene oxide was synthesis by using modified hummer's method. A 3 g of graphite flakes were dissolved in 10 ml of H_2SO_4, and then oxidizing agents $K_2S_2O_8$ and P_2O_5 were added to the mixture and stirred at 90 °C till the flakes were dissolved. The stirring continued for 4 more hours at 80 °C and the solution was then diluted with 500 ml of double distilled water. After the dilution, the solution was stirred overnight, filtered, washed with double distilled water and then dried to get the powdered form of graphene oxide. Pre-oxidized graphene powder was then subjected to further oxidation with 125 ml of H_2SO_4 and 15g of potassium permanganate ($KMnO_4$) in an ice bath where the solution was stirred for 2 h. Then, 130 ml of double distilled water was added to the mixture and this caused the temperature to rise to 95 °C. After 15 min, 15 ml of hydrogen peroxide (30%, v/v) was added to reduce the manganese in the solution to manganese sulphate (Mn→ $MnSO_4$). Finally, the solution was diluted with 400 ml of double distilled water and resultant yellow suspension was stirred overnight. The GO was filtered and washed thoroughly with NaOH and water till the rinsed water pH was found to be approximately 7.

The following procedure was used to prepare magnetic graphene oxide (mGO) by solvothermal method. 0.5 g of GO were added to 75 ml Ethylene glycol and the mixture was ultra-sonicated for approximately 150 min in temperature 30°*C*. Then, 1.6 g of $FeCl_3{\cdot}6H_2O$ and 3.0 g of Sodium acetate were stirred for 40 min. The obtained mixture was transferred to Hydrothermal Autoclave Reactor and raised the temperature to 200°*C* for 8 h. The obtained black product was washed out repeatedly with diluted water and ethanol to remove extra particles.

2.2.2. Functionalizing of magnetic graphene oxide with EDTA

0.1 g of mGO with 50 mL ethanol were dispersed for 1 h. Then, 1.5 mmol of EDTA-silane was added to 20 mL of ethanol and the mixture was dispersed. The initiated mixture was added to the second mixture. The obtained mixture was stirred for 12 h (at 60°*C*) and the brownish solid (EDTA-silane/mGO) was separated by appropriate magnet. In this case, the trialkoxy groups of EDTA-silane were hydrolyzed with the hydroxyl and carboxyl groups on the surface of mGO and were created –Si-OH bonds. The reaction between C–OH functional groups on GO and generated –Si-OH created a Si–*O*–C band.

2.2.3. Functionalizing of EDTA-silane/mGO with chitosan

In the final stage of synthesis CS/EDTA-silane/mGO nano-bio-composite, the EDTA/mGO was functionalized with chitosan by deposition-crosslinking method. In this case, 1.0 g EDTA-silane/mGO and 1.0 g CS were added into 1000 mL of acetic acid (0.2%) and the mixture was stirred in shaker for 90 min. Then, mixture's pH was adjusted to 11 with adding ammonia solution 1.0% gradually and dropwise. Then, the temperature was raised until the mixture reaches constant temperature of 60°*C* to become prepared for adding 0.5 mL glutaraldehyde. Turning the mixture to present coagulate CS was successfully cross-linked to the EDTA-silane/mGO and mGO surface. The resultant was washed out with diluted acetic acid with pH of 4 in order to remove uncross-linked precipitate. Finally, the obtained CS/EDTA-silane/mGO was dried at 50°*C* by a vacuum oven.

The synthesis of CS/EDTA-silane/mGO nano-bio-composite is schematically illustrated in Fig. 1, generally obtained over four steps.

2.3. Characterization

The X-ray diffraction patterns were measured by (Philips-PW 17C diffractometer; Japan) ($2\theta = 10$ to 80°) (solid-state detector via Cu Kα radiation, 40 Kv, 40 mA). The FT-IR (Shimadzu 4600 spectrometer; Japan) was conducted to identify the functional groups on the surface of graphene oxide within the range of 400–4000 cm^{-1}. The surface morphology of graphene oxide was visualized by the surface scanning electron microscopy (SEM; LEO 1455VP; Cambridge, U.K.). The magnetic saturation of mGO, EDTA-silane/mGO and CS/EDTA-silane/mGO were measured by (VSM; Kashan, Iran) from the range of −1000 to 1000 O_e at 25 °*C* temperature.

2.4. Adsorption experiments

For comparative study of single and multi-component adsorption of heavy metal ions, two types of batch experiments were conducted. In order to study the performance of nano-bio-composite CS/EDTA-silane/

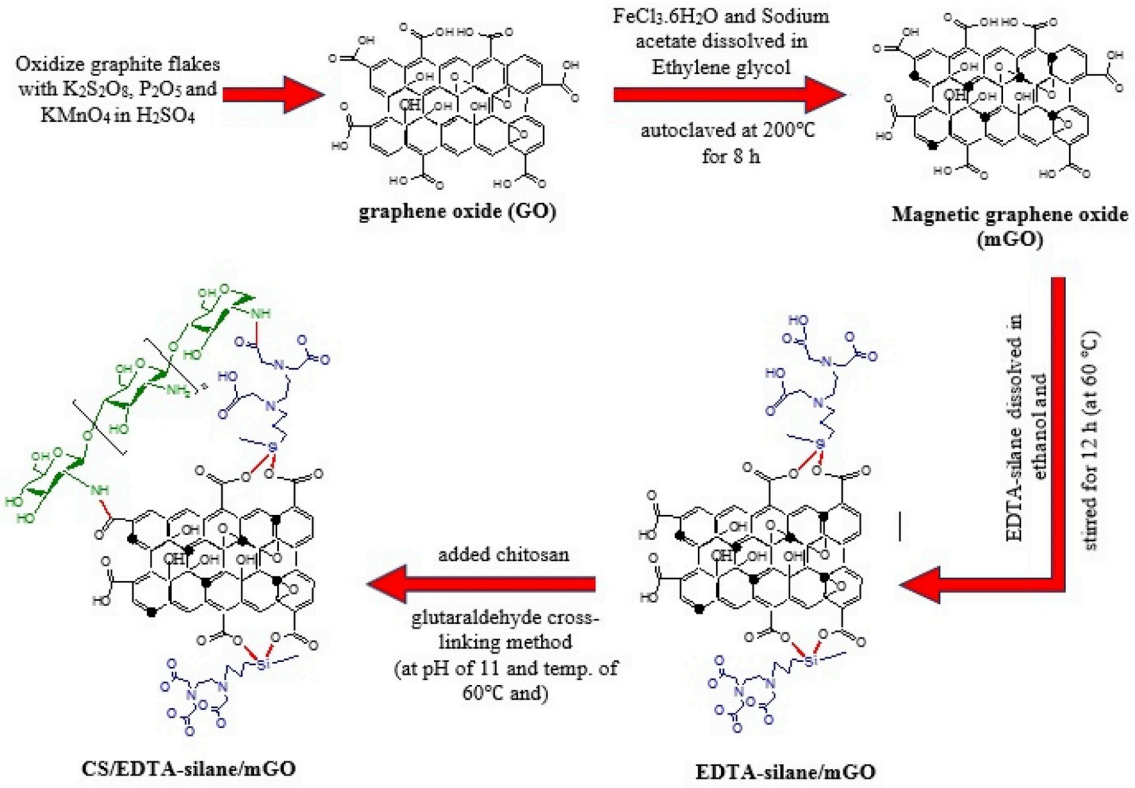

Fig. 1. Schematically illustration of synthesis of CS/EDTA-silane/mGO nano-bio-composite.

mGO in a single and binary, the standard solution of Pb(II) and Cd(II) were prepared at the room temperature. Before binary adsorption experiments, the effect of pH (range from 3 to 7) and sorbent dosage (from 0.2 to 0.6 g/L) were studied in single solution of Pb(II) and Cd(II) with concentration of 0.5 mmoL/L. For all experiments, the initial concentrations of Pb(II) and Cd(II) were considered as molar equivalently. Single and binary adsorption experiments were studied at dosage of adsorbent and pH of 0.3 g/L and 5, respectively. The kinetic experiments were achieved using 0.5 mmoL/L as initial concentration of metal ion single-component (t = 0–60 min). For studying thermodynamic nature of adsorption, the metal ion adsorption test was carried out at various temperatures (from 10 to 40°*C*).

For binary adsorption experiments, the ratios of metal concentration were selected as follow: Pb(II)/Cd(II) = 1:0, Pb(II)/Cd(II) = 0:1, Pb(II)/Cd(II) = 2:1, Pb(II)/Cd(II) = 1:1, Pb(II)/Cd(II) = 1:2. The final concentration of single and binary batch flasks were analyzed by atomic adsorption spectrometer. The removal percentage and adsorbent capacity in single-component batch adsorption experiments were calculated with equations (1) and (2), respectively (Salahshoor and Shahbazi, 2016; Mobarak et al., 2019):

$$(R\%) = \frac{(C_0 - C_e)}{C_0} \times 100 \quad (1)$$

$$(q_e) = \frac{(C_0 - C_e)}{M} \quad (2)$$

where C_0 is initial concentration of heavy metal ions (mg/L) and C_e is concentration of mixture in equilibrium (mg/L) at time *t* (min). M is sorbent dosage (g/L).

3. Results and discussion

3.1. Characterization

The surface morphology of synthesized graphene oxide is represented in Fig. 2a. This image exhibits a thin layer structure of graphene oxide (Achary et al., 2018). The several wrinkles which appeared in the sheet-like structure of graphene oxide can be explained by adding carboxyl, epoxy and hydroxyl functional groups. The mentioned functional groups can change the sp^2 (planner) structure of carbon to the sp^3 (tetrahedral) structure (İlbay et al., 2017; Marnani and Shahbazi, 2019).

The SEM image of CS/EDTA-silane/mGO is shown in Fig. 2b. According to Fig. 2b the morphology of graphene oxide has been conserved during its functionalization with EDTA and chitosan.

The saturation magnetization measurement of magnetic graphene oxide, EDTA-silane/mGO and CS/EDTA-silane/mGO can be observed in Fig. 3. The result of this measurement for mGO, EDTA-silane/mGO and CS/EDTA-silane/mGO are 44, 20 and 18 emu g^{-1}, respectively. Reduction in saturation magnetization value of mGO from 44 to 18 emu g^{-1} for CS/EDTA-silane/mGO can be explained by increasing total relative mass of nano-composite EDTA-silane/mGO and CS/EDTA-silane/mGO through functionalizing process (Ren et al., 2013; Marnani and Shahbazi, 2019). Although, the reduction value of saturation magnetization in nano-composite EDTA-silane/mGO and CS/EDTA-silane/mGO show that the amount of magnetic particle is appropriate. In addition, the product (CS/EDTA-silane/mGO) can get separated rapidly from aqueous solution with external magnetic field which is illustrated in Fig. 3-inside (Ren et al., 2013; Salahshoor and Shahbazi, 2016).

The diffraction pattern of GO, mGO, EDTA-silane/mGO and CS/EDTA-silane/mGO is demostrated in Fig. 4. The XRD diffraction peak at $2\theta = 10.57°$ is attributed to (002) reflection of GO which represent the appropriate organize sheet-like structure of synthesized graphene oxide with hummer's method (İlbay et al., 2017; Marnani and Shahbazi,

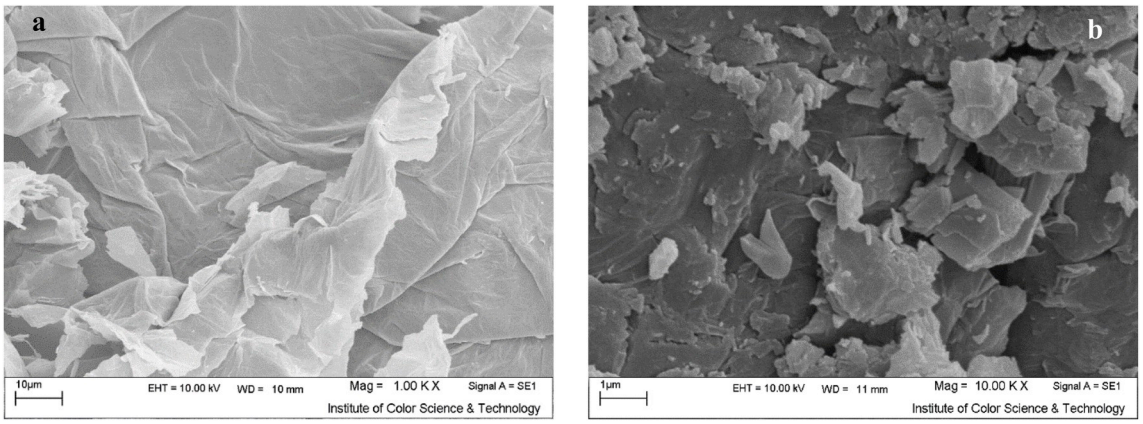

Fig. 2. The SEM image of GO and CS/EDTA-silane/mGO.

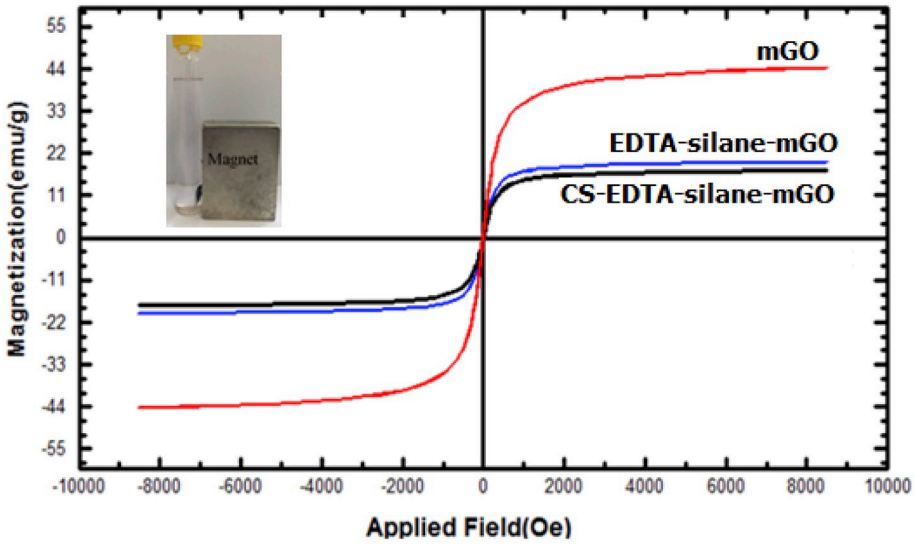

Fig. 3. The vibrating sample magnetometer (VSM) results (inside: magnetically separation of adsorbent from solution).

2019). Based on XRD data, the inter planer distance between graphene oxide layers was estimated 0.924 nm which confirmed extra hydroxyl, epoxy and carboxyl functional groups on the surface of GO (Wang et al., 2016; İlbay et al., 2017; Marnani and Shahbazi, 2019). The peaks at $2\theta = 31.1°$, 35.3°, 43.72°, 53.68°, 56.8° and 62.38° which correspond to (220), (311), (400), (422), (511) and (440) indicate the successful loading of magnetic particles on the surface of GO (Gupta et al., 2014; Zhao et al., 2016). The XRD pattern exhibits peak at $2\theta = 17.6°$ which assign to the EDTA (Zhao et al., 2016; Marnani and Shahbazi, 2019). Fig. 4 demonstrates a broad weak peak at $2\theta = 20°$ that confirm the presence of CS as a functional group in nano bio-composite CS/EDTA--silane/mGO (Li et al., 2013; Wang et al., 2014; Zhao et al., 2016).

The FT-IR spectra of mGO, EDTA-silane/mGO and CS/EDTA-silane/mGO are illustrated in Fig. 5. The strong peak at 1043 cm^{-1} is attributed to the C–O groups in carboxyl, hydroxyl and epoxy functional groups of graphene oxide (Xing et al., 2017). The peak located at 1219 cm^{-1} is corresponded to the stretching vibration of C–OH groups of carboxyl and hydroxyl groups (Xing et al., 2017; Marnani and Shahbazi, 2019). The peak at 1564 cm^{-1}relates to the stretching vibration of C═C which suggests aromatic structure of synthesized graphene oxide nano sheets (Shi et al., 2014). The C═O absorbance band is indicated at 1728 cm^{-1} which is assigned to –COOH functional groups of GO (Shi et al., 2014). The two peaks located at 3492 and 1643 cm^{-1} offer the presence of water molecules and stretching bands of O–H and H–*O*–H in the structure of carbon skeleton of graphene oxide.

The peaks at 457 and 572 cm^{-1} are attributed to the vibration of Fe–O which represents successful loading of magnetic nano particle on the surface of graphene oxide (Marnani and Shahbazi, 2019).

In the spectrum of EDTA-silane/mGO, a strong peak at 1101 cm^{-1} confirm the existence of Si–*O*–C bond and successful loading of EDTA-silane functional group on the surface of mGO. Also, a peak at 1415 cm^{-1} is corresponded to the C–N bond formation and the existence of EDTA-silane as a functional group. The advent of new bond at 2854 cm^{-1} is assigned to methylene groups of EDTA (Padilla-Ortega et al., 2013; Lv et al., 2018).

In the spectrum of CS/EDTA-silane/mGO, two peaks at 1230 and 1100 indicate the C–N stretching vibration of $–NH_2$ which are the result of existence of CS on the surface of EDTA-silane/mGO nano composite. Further, the peak located at 1579 cm^{-1} could be ascribed to secondary amine groups –NH groups which exhibit the interaction between amine and epoxy functional groups (Yan et al., 2016; Marnani and Shahbazi, 2019).

3.2. Adsorption experimental results

3.2.1. The effect of pH

The results of the effect of pH on adsorption is shown in Fig. 6. The appropriate pH seems to be 5 for both studies metal ions which causes the greatest ion removal. In this pH, 77 and 28% of Pb(II) and Cd(II),

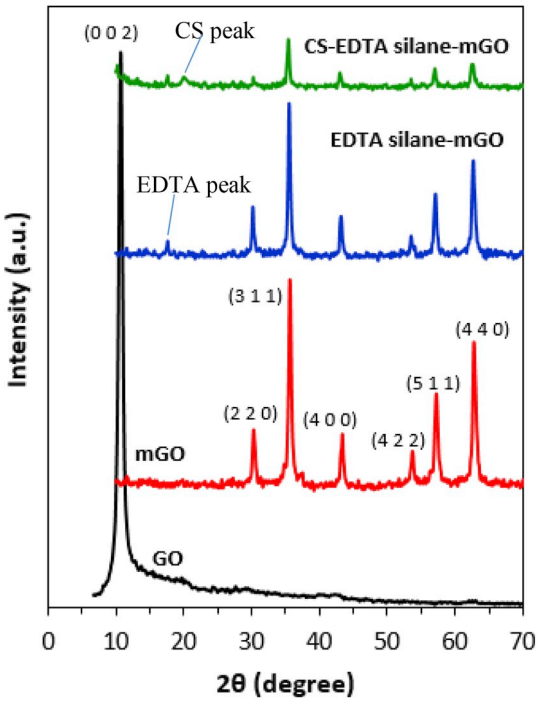

Fig. 4. The XRD pattern of synthesis materials.

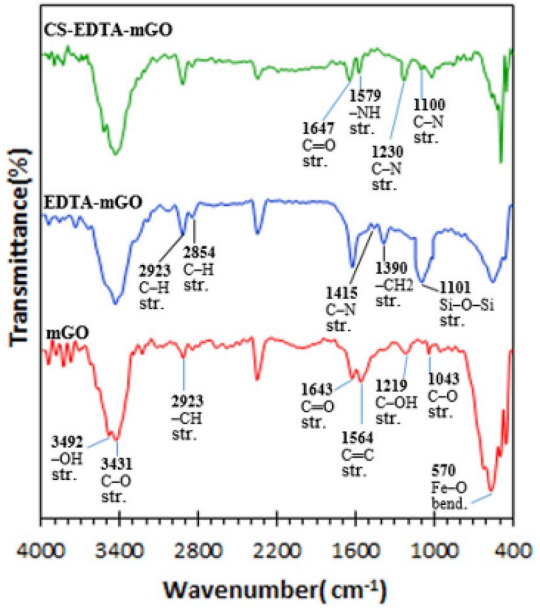

Fig. 5. The FTIR spectrums of synthesis materials.

respectively, was removed from single solution with initial concentration of 0.5 mmoL/L of metal ion and adsorbent dosage of 0.2 g/L. According to literature, the adsorption of metal ions is clearly regarding to pH. The decrease in metal ions removal with the increase in pH could be explained by the rapid changes between protonated and deprotonated forms of the amine and carboxyl groups of chitosan and EDTA (Soetaredjo et al., 2013; Muhana et al., 2017; Liu et al., 2018). Hence, there is a possibility of precipitation of metal ions as metal hydroxides at pH values higher than 5. The precipitates of hydroxides metals, tend to re-dissolve as pH increase beyond the 5. At high acidic pH condition, protonation of amine groups (e.g. $NH_2 \rightarrow NH_3^+$) causes in diminishing of metal adsorption. Therefore, the number of active sites and

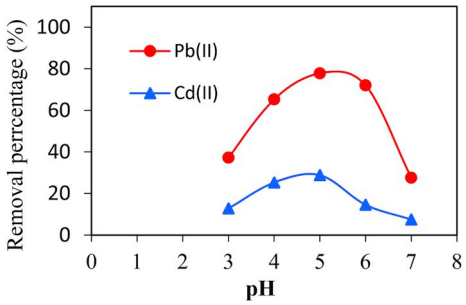

Fig. 6. The effect of pH and adsorbent dosage on single-metal ion removal ($C_0 = 0.5$ mmoL/L; adsorbent dosage = 0.2 g/L).

consequently the R% reduce.

3.2.2. *The effect of adsorbent dosage*

The effect of adsorbent dosage was studied at pH of 5 and initial single metal ion concentration of 0.5 mmoL/L. The results of adsorbent dosage are shown in Fig. 7. The removal percentage of metal ions increases with increasing the adsorbent dosage. However, the entire ion removal (100%) is observed at 0.4 and 0.5 g/L for Pb(II) and Cd(II), respectively. While according to adsorption capacity (q_e), the adsorbent dosage of 0.3 g/L was selected for subsequent studies. On the other hands, the more active sites were used at a lower adsorbent dosage (Mobasherpour et al., 2012; Luo et al., 2015).

3.2.3. *Adsorption kinetic (single-component)*

The kinetic parameters including the correlation coefficient (R^2), predicted q_e and kinetic constant, which are determined from the fitting results, are shown in Table 1. The adsorption proceeded rapidly and reached to the equilibrium at 30 and 40 min for Pb(II) and Cd(II), respectively. As shown in Fig. 8 and Table 1, the pseudo-first-order model is more suitable for simulating the adsorption kinetics not only due to its high correlation coefficient (R^2), but also its closest predicted q_e value to q_e which was obtained from experimental data. In addition,

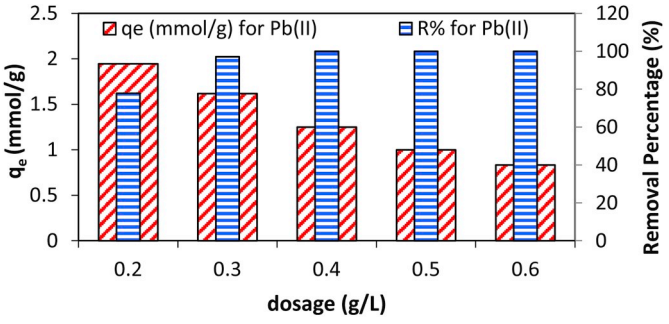

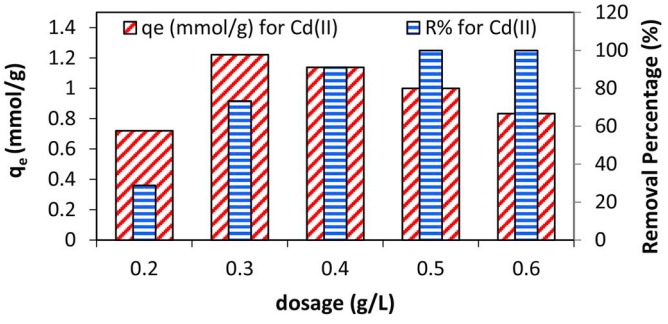

Fig. 7. The effect of adsorbent dosage on single-metal ion removal ($C_0 = 0.5$ mmoL/L; pH = 5).

Table 1
Kinetics parameters for Pb(II) and Cd(II) adsorption onto CS/EDTA-silane/mGO from single-component.

Metal ion	Pseudo-first-order kinetic			Pseudo-second-order kinetic		
	k_1, min^{-1}	q_{e1}, mmol/g	R^2	k_2, g/mmol min	q_{e2}, mmol/g	R^2
Pb(II)	0.2145	2.2474	0.9979	0.1174	2.5040	0.9909
Cd(II)	0.0815	1.0627	0.9981	0.0599	1.3257	0.9897

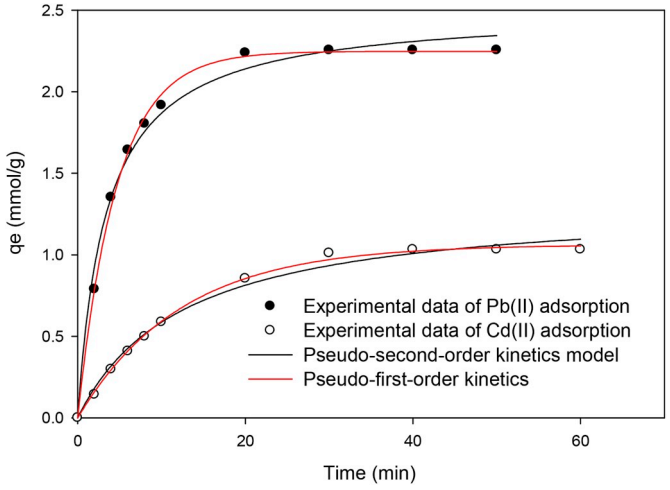

Fig. 8. Adsorption kinetics modeling of Pb(II) and Cd(II) onto Cs/EDTA-silane/mGO from single-component (pH = 5; adsorbent dosage of 0.3 g/L; C_0 = 0.5 mmoL/L).

the adsorption rate of Pb(II) is 2.6 times higher than that for Cd(II) ions. The higher sorption kinetic rate for Pb(II) could be due to Pb(II) 's smaller hydrated radius in comparison to Cd(II) ions (Pb(II) = 0.401 nm vs. Cd(II) = 0.426 nm). The other reason for affinity could be the higher electronegativity of Pb(II) than that of Cd(II) (Mobasherpour et al., 2012; Gupta et al., 2014; Luo et al., 2015).

3.2.4. Adsorption thermodynamic (single-component)

The effect of temperature variation (283, 293, 303, and 313 K) on the adsorption performance of CS/EDTA-silane/mGO were conducted to evaluate the mechanisms involved in the adsorption process. The van't Hoff equations (Eqs. (3) and (4)) were applied for determining the free energy change (ΔG, kJ/mol), entropy change (ΔS, J/mol K), and enthalpy change (ΔH, kJ/mol) (Salahshoor and Shahbazi, 2016).

$$\Delta G = \Delta H - T\Delta S \tag{3}$$

$$\ln K_d = \frac{\Delta S}{R} - \frac{\Delta H}{RT} \tag{4}$$

where, T is the temperature (K), K_d represents the thermodynamic equilibrium constant (L/g), and R shows the universal gas constant (8.13 J/mol K). ΔH and ΔS are predicted from the slope and intercept of the linear plot of lnK *vs.* 1/T, respectively (Fig. 9).

The values of ΔG for mertal ion adsorption onto CS-EDTA-mGO in single adsorption experiment at temperatures of 10, 20, 30, and 40 °C were calculated as −53.0, −54.9, −56.8, and 58.6 kJ/mol for Pb(II), and −37.7, −39.1, −40.4, and −41.8 kJ/mol for Cd(II), respectively. The feasibility and spontaneity of the adsorption process was approved by the negative sign of ΔG. Furthermore, the ascending negative value of ΔG by elevating temperature confirmed the favorability of sorption process at higher temperatures. Also, the positive sign of ΔH (0.051 kJ/mol for Pb(II) and 0.037 kJ/mol for Cd(II)) indicated that the interaction of solid-solution was endothermic. The magnitude of ΔH gives information about the types of adsorption. In physisorption, development of bond between the adsorbate molecule and active sites on the adsorbent requires low energy, hence the value of enthalpy is usually not beyond 4.2 kJ/mol (Salahshoor and Shahbazi, 2016). The positive value of ΔS (187.5 J/mol K for Pb(II) and 133.5 J/mol K for Cd(II)) implies that through the adsorption of metal ions onto CS/EDTA-silane/mGO, the disorder and randomness increased at the solid-solution interface.

3.2.5. Isotherm studies (single and multi-component)

The results of isotherm studies in binary system are shown in Fig. 10. The effect of the existence of Pb(II) on Cd(II) removal seems to be robust and significant. In the single-component condition (Pb(II)/Cd(II) = 0:1), the experimental adsorption capacity for Cd(II) is 1.05 mmoL/g. However, in the presence of Pb(II) with the same molar concentration (Pb(II)/Cd(II) = 1:1), the above value strongly decreases to 0.66 mmoL/g (37% decrease). In the more sever condition in which the concentration of Pb(II) was two times higher than Cd(II) (Pb(II)/Cd(II) = 2:1), the removal percentage of removal shows 48% decreases comparing to the single-component condition of Cd(II) (0.55 vs. 1.05 mmoL/g) (Soetardjo et al., 2013).

The effect of the co-existence Cd(II) on Pb(II) adsorption onto CS/EDTA-silane/mGO was found to be negligible as illustrated in Fig. 10. In the case of single-component solution (Pb(II)/Cd(II) = 1:0), the experimental adsorption capacity of Pb(II) was 2.32 mmoL/g which is 2.22 times higher than this value for Cd(II) in single-component solution (Mobasherpour et al., 2012). Therefore, the affinity of CS/EDTA-silane/mGO for adsorption of Pb(II) is much higher than this affinity for Cd(II). It could be due to the fact that Pb(II) has smaller

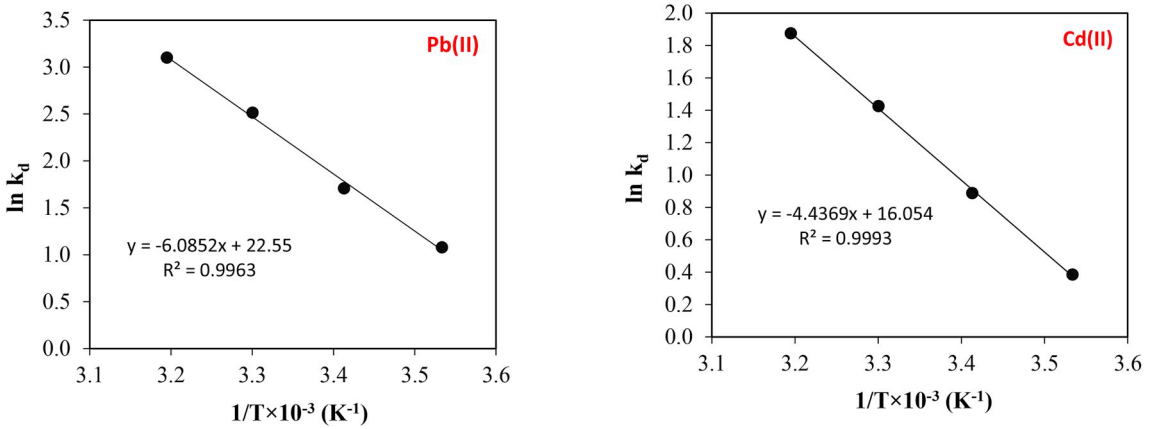

Fig. 9. Van't Hoff plot for adsorption of Pb(II) and Cd(II) onto CS/EDTA-silane/mGO from single aqueous solution.

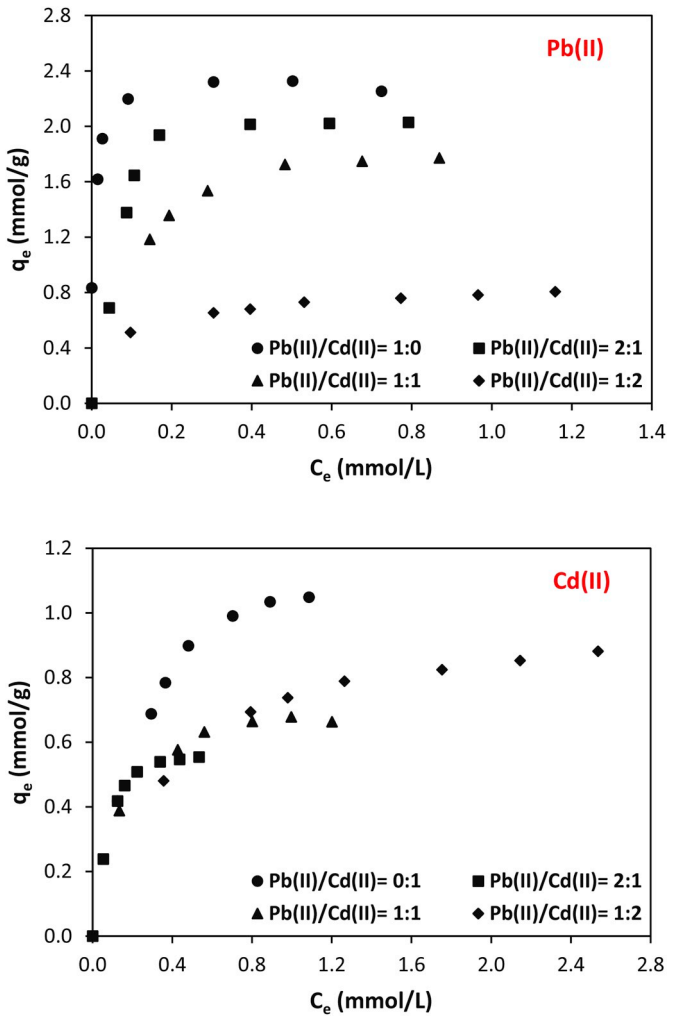

Fig. 10. Isotherms (raw and unfitted data) for the adsorption onto CS/EDTA-silane/mGO from a binary aqueous solution with different initial molar ratios of Pb(II) and Cd(II).

hydrated radius and higher electronegativity compared with Cd(II) (Padilla-Ortega et al., 2013; Soetaredjo et al., 2013). Hence, the Pb(II) ions was adsorbed easier than Cd(II) onto adsorbent.

In the presence of Cd(II) ions with equal molar concentration (Pb(II)/Cd(II) = 1:1), the above value slightly decreased to 1.77 mmoL/g. However, nearly negligible decreasing of adsorption capacity was observed (only 9%) at molar ratio of Pb(II)/Cd(II) = 2:1 compared to Pb (II)component solution.

Pb(II) and Cd(II) species in the solution have interaction during bi-component adsorption which could be varied from full competition to synergism or independence. The type of effects, i.e., synergism, antagonism and non-interaction can be explained by calculating the ratio of adsorption capacity ($Rq,i = q_{mix,i}/q_{0,i}$) as follow:

(1) Synergism ($q_{mix,i}/q_{0,i} > 1$): effect of mixture of component in solution is greater than its individual effect;
(2) Antagonism ($q_{mix,i}/q_{0,i} < 1$): effect of mixture of component in solution is less than its individual effect;
(3) Non-interaction ($q_{mix,i}/q_{0,i} = 1$): effect of mixture of component in solution is neither less nor more than that of its individual effect; where, q_{mix} is the adsorption capacity of one component in the binary solution and q_0 is the adsorption capacity when presents single.

The results of the calculation of q_{mix}/q_0 for Pb(II) and Cd(II) are summarized in Table 2.

As observed the value of q_{mix}/q_0 for Cd(II) decrease to lower than 1 along with the increase of Pb(II)/Cd(II) ratio to 2:1, exhibiting in case a antagonism/inhibition effect contrary to almost non-interaction effect at same concentration of metal ions in the solution. The effect of Pb(II) on Cd(II) adsorption in the binary solution shift to synergetic when the concentration of Cd(II) is two times higher than the concentration of Pd (II) (Pb(II)/Cd(II) 1:2), hence, no competition was observed between Pb (II) and Cd(II) during simultaneous adsorption at low concentration of Pb(II). This could be explained with the fact that at lower molar ratio of Cd(II) even at the same molar ratio of Pb(II) and Cd(II), the Pb(II) ions overcome to occupy the adsorption sites due to their (i) higher electronegativity; (ii) higher adsorption rate (2.6 times); (iii) higher metal diffusivity properties and adsorption affinity compare to Cd(II) (Jiu-Hua Deng et al., 2013).

For Pb(II) adsorption in binary solution, according to value of q_{mix}/q_0 (>1) it concludes that the presence of Cd(II) at any studied molar ratio doesn't have any antagonistic effect on Pb(II) adsorption. So, in the range of studied concentration and molar ratios, the concentration of Cd (II) has synergistic effect on Pb(II) adsorption.

For identifying the affinity of adsorbent for each metal ion, the adsorption selectivity ($S_i = q_{e,metal1}/q_{e,metal2}$) of heavy metals on CS/EDTA-silane/mGO in binary solutions were calculated and summarized in Table 2. According to the results, in the same metal ion molar concentration (Pb(II)/Cd(II) = 1:1), the CS/EDTA-silane/mGO shows more affinity for adsorption of Pb(II) which is more than 2.6 times compared to Cd(II) (2.67 vs. 0.37). For both metal ions, when the molar ratio increases to 2, the CS/EDTA-silane/mGO offers more affinity for the adsorption of metal ion with more concentration. However, in this case the affinity of CS/EDTA-silane/mGO for adsorption of Pb(II) is 3.6 times higher than that for Cd(II).

3.2.6. Binary isotherm modeling

The isotherms of binary sturdies were evaluated and modeled using several well-known predictive and correlative models listed in Table 3.

The results of binary isotherm modeling are summarized in Table 4. Also, the suitably of fitted models were evaluated by calculation of F_{obj} (objective function) involving experimental and calculated adsorption capabilities ($q_{e,exp}$ and $q_{e,calc}$, respectively) which is based on relative least-squares (Eq. (5)). The fitted model with lower value for objective function leads to the lowest difference between $q_{e,exp}$ and $q_{e,calc}$ which subsequently results in the better prediction and interpretation of experimental data.

$$F_{obj} = \sum_{j=1}^{n}\left[\sum_{i=1}^{c}\left(\frac{q_{e,i}^{exp} - q_{e,i}^{calc}}{q_{e,i}^{exp}}\right)_j^2\right] \quad (5)$$

3.3. Comparison of adsorption properties

For evaluation of the maximum adsorption capacity of CS/EDTA-silane/mGO for Pb(II) and Cd(II) compared to similar sorbents, the data and results of similar studies are presented in Table 5.

Sitko et al. (2013) used graphene oxide for adsorption of divalent metal ions from aqueous solutions and found the maximum sorption capacity of 269 and 126 mg/g for Pb(II) and Cd(II), respectively. A

Table 2
The results of the calculation of q_{mix}/q_0 and adsorption selectivity for Pb(II) and Cd(II).

Ratios of metal concentration	$R_{q,i}$		S_i	
	$R_{q,Pb(II)}$	$R_{q,Cd(II)}$	$S_{Pb(II)}$	$S_{Cd(II)}$
Pb(II)/Cd(II) = 2:1	2.46	0.72	3.66	0.27
Pb(II)/Cd(II) = 1:1	2.32	0.99	2.67	0.37
Pb(II)/Cd(II) = 1:2	1.09	1.72	0.92	1.09

Table 3
Binary isotherm models and parameters.

Binary isotherm model	formula	parameter
Extended Langmuir	$q_{e,i} = \frac{q_{max} K_i C_{e,i}}{1 + \sum_{j=1}^{c} K_j C_{e,j}}$	q_{max} is maximum adsorption capacity of adsorbent.
Non-modified Langmuir	$q_{e,i} = \frac{q_{m,i} K_{L,i} C_{e,i}}{1 + \sum_{j=1}^{c} K_{L,j} C_{e,j}}$	$q_{m,i}$ is maximum adsorption capacity for component i. K is Langmuir isotherm constant in multicomponent (L/g) for each component. C_e is equilibrium liquid-phase concentration (mmol/L) for each component.
Extended Freundlich	$q_{e,1} = \frac{K^0_{F,1} C_{e,1}^{n_1+n_{11}}}{C_{e,1}^{n_{11}} + a_{12} C_{e,2}^{n_{12}}} q_{e,2} = \frac{K^0_{F,2} C_{e,2}^{n_2+n_{22}}}{C_{e,2}^{n_{22}} + a_{21} C_{e,1}^{n_{21}}}$	$n_{i,j}$ ($n_{1,1}$, $n_{1,2}$, $n_{2,2}$, $n_{2,1}$, $a_{1,2}$ and $a_{2,1}$) is dimensionless correlative constants obtained by experimental binary data of components 1 and 2, respectively. $K_{F,i}$ is dimensionless extended Freundlich isotherm constant. $C_{e,i}$ is equilibrium liquid-phase concentration (mmol/L).

Table 4
The constants and coefficients of studied binary isotherm (1 and 2 are related to Pb(II) and Cd(II), respectively).

Model	parameter and constants	Binary condition		
		Pb(II)/Cd (II) = 2:1	Pb(II)/Cd (II) = 1:1	Pb(II)/Cd (II) = 1:2
Extended Langmuir	q_{max} (mmol/g)	3.00	2.80	2.00
	K_1 (L/g)	1.00	0.81	0.50
	K_2 (L/g)	0.97	0.41	0.52
	F_{obj}	4.13	3.20	3.64
Non-modified Langmuir	$q_{m,1}$ (mmol/g)	3.0	3.00	2.61
	$q_{m,2}$ (mmol/g)	3.0	2.53	3.21
	$K_{L,1}$ (L/g)	1.0	1.0	0.90
	$K_{L,2}$ (L/g)	0.97	0.49	0.34
	F_{obj}	4.12	3.01	3.21
Extended Freundlich	n_1	0.0000	0.0005	0.0001
	n_2	0.8920	0.4235	0.4523
	$n_{1,1}$	1.0000	0.9623	0.8984
	$n_{2,2}$	0.0008	0.0004	0.0076
	$n_{1,2}$	0.0000	0.0846	0.0084
	$n_{2,1}$	0.5704	0.9990	0.8696
	$a_{1,2}$	0.0878	0.1168	0.1212
	$a_{2,1}$	7.2835	0.5708	0.6957
	$K_{F,1}$	2.4596	2.0596	2.0564
	$K_{F,2}$	7.2800	0.9293	1.0026
	F_{obj}	0.120	0.003	0.004

Best data adjustment (the lowest F_{obj} value) was found from extended Freundlich model in which a heterogeneously surface is considered.

maximum sorption capacity of 91.2 mg/g was approximately predicted for Cd(II) with magnetic graphene oxide (Dorabei et al., 2016).

Carpio, mangaldao et al. (2014) were synthesized EDTA-GO and evaluated its adsorption capacity for two heavy metals, Pb(II) and Cd (II). The maximum adsorption capacity of the GO–EDTA was determined to be 454 mg/g and 108 mg/g for Pb(II) and Cu(II), respectively. They approved that the GO–EDTA did not present any cytotoxicity to human corneal epithelial cells. The modified graphene oxide with 2,2′-Dipyridylamine showed maximum sorption capacity of about 369.7 and 97.2 mg/g for Pb(II) and Cd(II), respectively (Zare-Dorabei, Ferdowsi et al. 2016). Li, Zhou et al. (2015) reported q_{max} of 407.0 mg/g for Pb(II) and 85.9 mg/g for Cd(II) by using chitosan/sulfydryl-functionalized graphene oxide. The use of magnetic chitosan/EDTA for heavy metals and dye removal was resulted in a q_{max} of 189.6 and 151.9 mg/g for Pb (II) and Cd(II), respectively (Chen et al., 2019).

Table 5
Comparison of maximum adsorption capacity of CS/EDTA-silane/mGO with similar reported adsorbent for Pb(II) and Cd(II) removal.

Adsorbent	adsorbate	q_{max} (mg/g)	pH of solution	Ref.
magnetic graphene oxide (mGO)	Pb(II)	319.5	5	This study
	Cd(II)	73.5		
EDTA-silane/mGO	Pb(II)	414.1	5	This study
	Cd(II)	93.3		
CS/EDTA-silane/mGO	Pb(II)	483.3	5	This study
	Cd(II)	118.0		
graphene oxide	Pb(II)	269.0	5	Sitko et al. (2013)
	Cd(II)	126.1		
	Cu(II)	294.4		
	Zn(II)	345.1		
magnetic graphene oxide	Cd(II)	91.2	_	Dorabei et al., 2016
	Methylene blue	64.2		
	Orange G	20.8		
EDTA-GO	Pb(II)	454.6	3	Carpio, mangaldao et al., 2014
	Cu(II)	108.7	5	
graphene oxide modified with 2,2′-Dipyridylamine	Pb(II)	369.7	5	Dorabei et al. (2016)
	Cd(II)	97.2		
	Ni(II)	180.8		
	Cu(II)	358.8		
chitosan/sulfydryl-functionalized graphene oxide	Pb(II)	407.9	5	Li et al., 2015a, b
	Cd(II)	85.9		
	Cu(II)	177.3		
magnetic chitosan/EDTA	Pb(II)	189.6	6	Chen et al. (2019)
	Cu(II)	151.9		
	Methylene blue	148.1		
EDTA functionalized bamboo activated carbon	Pb(II)	114.9	5	Lv et al. (2018)
	Cu(II)	39.6		
bentonite-chitosan	Pb(II)	63.2	6	Sellaoui et al. (2018)
	Cd(II)	77.1		

In the current study, modification of magnetic graphene oxide with chitosan and EDTA showed a high maximum sorption capacity of 483.3 and 118.0 mg/g for Pb(II) and Cd(II), respectively. According to Table 5, the adsorption capacity of CS/EDTA-silane/mGO increases 33 and 38% comparing to mGO for Pb(II) and Cd(II), respectively. Based on these comparisons, it can be concluded that CS/EDTA-silane/mGO provides a promising magnetic nano-adsorbent for the removal of Pb(II) and Cd(II) ions.

4. Conclusion

In this study, multi-functionality of graphene oxide nanomaterials with amine-containing groups (chitosan and EDTA) was developed for adsorption of Pb(II) and Cd(II) heavy metal ions in single- and binary-system. The first-second-order kinetic model found to provide the closest fit to the data for kinetic studies of single system (R^2= 0.998; $k_1 = 0.2145\ min^{-1}$ is for Pb(II) and $R^2 = 0.998$; $k_1 = 0.0815\ min^{-1}$ is for Cd(II)). The results confirm that the adsorption of Pb(II) and Cd(II) onto CS/EDTa-sinane/mGO were endothermic and spontaneous; thus, the amount of adsorbed ions increased as temperature increased. The results indicated that the maximum adsorption capacity of CS/EDTa-sinane/mGO for Pb(II) and Cd(II) is 2.33 and 1.05 mmoL/g, respectively, in single system. According to the results, the higher electro valence and the smaller ion radius of Pb(II) lead CS/EDTa-sinane/mGO to higher adsorption capacity for Pb(II) with easier adsorption reactions, which makes higher kinetic rate, compared with Cd(II) adsorption. The interactive effect of binary-metal ions in binary component systems with same ion concentration was almost non-interaction, even though, by increasing the molar ratio of each metal ion, the interactive effect depends on metal physiochemical properties. On the other hand, the simultaneous presence of Pb(II) and Cd(II) in aqueous solutions reduced the Cd(II) adsorption capacity, while there was limited effect on

adsorption capacity of Pb(II). CS/EDTA-silane/mGO produces (or provides) a promising magnetic nano-adsorbent for the removal of Pb(II) and Cd(II) ions compared with similar adsorbents.

Acknowledgments

The authors would like to thank the Iran Nanotechnology Initiative Council (INIC) for their financial support (grant number: 116395). Also, we would like to appreciate Shahid Beheshti University for laboratory supports.

References

Achary, L.S.K., Kumar, A., Rout, L., Kunapuli, S.V., Dhaka, R.S., Dash, P., 2018. Phosphate functionalized graphene oxide with enhanced catalytic activity for Biginelli type reaction under microwave condition. Chem. Eng. J. 331, 300–310.

Beheshti, H., Irani, M., Hosseini, L., Rahimi, A., Aliabadi, M., 2016. Removal of Cr (VI) from aqueous solutions using chitosan/MWCNT/Fe 3 O 4 composite nanofibers-batch and column studies. Chem. Eng. J. 284, 557–564.

Carpio, I.E., Mangadlao, M.J.D., Nguyen, H.N., Advincula, R.C., Rodrigues, d.F., 2014. Graphene oxide functionalized with ethylenediamine triacetic acid for heavy metal adsorption and anti-microbial applications. Carbon 77, 289–301.

Chen, B., Zhao, H., Chen, S., Long, F., Huang, B., Yang, B., Pan, X., 2019. A magnetically recyclable chitosan composite adsorbent functionalized with EDTA for simultaneous capture of anionic dye and heavy metals in complex wastewater. Chem. Eng. J. 356, 69–80.

Dorabei, R.Z., Ferdowsi, S.M., Barzin, A., Tadjarodi, A., 2016. Highly efficient simultaneous ultrasonic-assisted adsorption of Pb(II), Cd(II), Ni(II) and Cu (II) ions from aqueous solutions by graphene oxide modified with 2,2-dipyridylamine: central composite design optimization. Ultrason. Sonochem. 32, 265–276.

Gupta, V.K., Atar, N., Yola, M.L., Üstündağ, Z., Uzun, L., 2014. A novel magnetic Fe@ Au core–shell nanoparticles anchored graphene oxide recyclable nanocatalyst for the reduction of nitrophenol compounds. Water Res. 48, 210–217.

Gupta, V.K., Nayak, A., Agarwal, S., Tyagi, I., 2014. Potential of activated carbon from waste rubber tire for the adsorption of phenolics: effect of pre-treatment conditions. J. Colloid Interface Sci. 417, 420–430.

Hou, S., Su, S., Kasner, M.L., Shah, P., Patel, K., Madarang, C.J., 2010. Formation of highly stable dispersions of silane-functionalized reduced graphene oxide. Chem. Phys. Lett. 501 (1–3), 68–74.

Huang, D., Wu, J., Wang, L., Liu, X., Meng, J., Tang, X., Tang, C., Xu, J., 2019. Novel insight into adsorption and co-adsorption of heavy metal ions and an organic pollutant by magnetic graphene nanomaterials in water. Chem. Eng. J. 358, 1399–1409.

İlbay, Z., Haşimoğlu, A., Özdemir, O.K., Ateş, F., Şahin, S., 2017. Highly efficient recovery of biophenols onto graphene oxide nanosheets: valorisation of a biomass. J. Mol. Liq. 246, 208–214.

Jiu-Hua Deng, J.H., Zhang, X.R., Zeng, G.M., Gong, J.L., Niu, Q.Y., Liang, J., 2013. Simultaneous removal of Cd(II) and ionic dyes from aqueous solution using magnetic graphene oxide nanocomposite as an adsorbent. Chem. Eng. J. 266, 189–200.

Kyzas, G.Z., Siafaka, P.I., Pavlidou, E.G., Chrissafis, K.J., Bikiaris, D.N., 2015. Synthesis and adsorption application of succinyl-grafted chitosan for the simultaneous removal of zinc and cationic dye from binary hazardous mixtures. Chem. Eng. J. 259, 438–448.

Li, Y., Du, Q., Liu, T., Peng, X., Wang, J., Sun, J., Wang, Y., Wu, S., Wang, Z., Xia, Y., 2013. Comparative study of methylene blue dye adsorption onto activated carbon, graphene oxide, and carbon nanotubes. Chem. Eng. Res. Des. 91 (2), 361–368.

Li, L., Wang, Z., Ma, P., Bai, H., Dong, W., Chen, M., 2015. Preparation of polyvinyl alcohol/chitosan hydrogel compounded with graphene oxide to enhance the adsorption properties for Cu (II) in aqueous solution. J. Polym. Res. 22 (8), 1–10.

Li, X.H., Zhou, W., Wu, S., Wei, Y., Xu, Y., Kuang, 2015. Studies of heavy metal ion adsorption on Chitosan/Sulfydryl- functionalized graphene oxide composites. Journal of Colloid and Interface Scienese 448, 389–397.

Liu, X., Liu, M., Zhang, L., 2018. Co-adsorption and sequential adsorption of the co-existence four heavy metal ions and three fluoroquinolones on the functionalized ferromagnetic 3D NiFe2O4 porous hollow microsphere. J. Colloid Interface Sci. 511, 135–144.

Luo, X., Zhang, Z., Zhou, P., Liu, Y., Ma, G., Lei, Z., 2015. Synergic adsorption of acid blue 80 and heavy metal ions (Cu2+/Ni2+) onto activated carbon and its mechanisms. J. Ind. Eng. Chem. 27, 164–174.

Lv, D., Liu, Y., Zhou, J., Yang, K., Lou, Z., Baig, S.A., Xu, X., 2018. Application of EDTA-functionalized bamboo activated carbon (BAC) for Pb (II) and Cu (II) removal from aqueous solutions. Appl. Surf. Sci. 428, 648–658.

Madadrang, C.J., Kim, H.Y., Gao, G., Wang, N., Zhu, J., Feng, H., Gorring, M., Kasner, M. L., Hou, S., 2012. Adsorption behavior of EDTA-graphene oxide for Pb (II) removal. ACS Appl. Mater. Interfaces 4 (3), 1186–1193.

Marnani, N.N., Shahbazi, A., 2019. A novel environmental-friendly nanobiocomposite synthesis by EDTA and chitosan functionalized magnetic graphene oxide for high removal of Rhodamine B: adsorption mechanism and separation property. Chemosphere 218, 715–725.

Mobarak, M., Mohamed, E.A., Selim, A.Q., Sellaoui, L., Lamine, A.B., Erto, A., Bonilla-Petriciolet, A., Seliem, M.K., 2019. Surfactant–modified serpentine for fluoride and Cr (VI) adsorption in single and binary systems: experimental studies and theoretical modeling. Chem. Eng. J. 369, 333–343.

Mobasherpour, I., Salahi, E., Pazouki, M., 2012. Comparative of the removal of Pb2+, Cd2+ and Ni2+ by nano crystallite hydroxyapatite from aqueous solutions: adsorption isotherm study. Arabian Journal of Chemistry 5 (4), 439–446.

Muhana, F.J., El-Eswed, B.I., Khalili, F.I., 2017. Synthesis of immobilized chitosan/humic acid coupling product for removal of Pb (II), Cd (II) and Cr2O72-from aqueous solutions. Desalination and Water Treatment 87, 292–305.

Padilla-Ortega, E., Leyva-Ramos, R., Flores-Cano, J., 2013. Binary adsorption of heavy metals from aqueous solution onto natural clays. Chem. Eng. J. 225, 535–546.

Ren, Y., Abbood, H.A., He, F., Peng, H., Huang, K., 2013. Magnetic EDTA-modified chitosan/SiO 2/Fe 3 O 4 adsorbent: preparation, characterization, and application in heavy metal adsorption. Chem. Eng. J. 226, 300–311.

Ren, Y., Chen, Y., Sun, M., Peng, H., Huang, K., 2014. Rapid and efficient removal of cationic dyes by magnetic chitosan adsorbent modified with EDTA. Separ. Sci. Technol. 49 (13), 2049–2059.

Salahshoor, Z., Shahbazi, A., 2016. Modeling and optimization of cationic dye adsorption onto modified SBA-15 by application of response surface methodology. Desalination and Water Treatment 57 (29), 13615–13631.

Saleh, T.A., Gupta, V.K., 2014. Processing methods, characteristics and adsorption behavior of tire derived carbons: a review. Adv. Colloid Interface Sci. 211, 93–101.

Sellaoui, L., Soetaredjo, F.E., Ismadji, S., Bonilla-Petriciolet, A., Belver, C., Bedia, J., Lamine, A.B., Erto, A., 2018. Insights on the statistical physics modeling of the adsorption of Cd2+ and Pb2+ ions on bentonite-chitosan composite in single and binary systems. Chem. Eng. J. 354, 569–576.

Shahbazi, A., Zonoz, F.B., 2015. Decolorization of Malachite green dye from wastewater by Populus deltoides: three-level Box–Behnken design optimization, equilibrium, and kinetic studies. Journal of Water Reuse and Desalination 5 (3), 250–263.

Shi, H., Li, W., Zhong, L., Xu, C., 2014. Methylene blue adsorption from aqueous solution by magnetic cellulose/graphene oxide composite: equilibrium, kinetics, and thermodynamics. Ind. Eng. Chem. Res. 53 (3), 1108–1118.

Sitko, R., Gagor, A., Turek, E., Feist, B., Zawisza, B., Malicka, E., Wrzalik, R., 2013. Adsorption of divalent metal ions from aqueous solutions using graphene oxid. Dalton Trans. 42, 5682–5689.

Soetaredjo, F.E., Kurniawan, A., Ki, O.L., Ismadji, S., 2013. Incorporation of selectivity factor in modeling binary component adsorption isotherms for heavy metals-biomass system. Chem. Eng. J. 219, 137–148.

Wang, S., Zhai, Y.-Y., Gao, Q., Luo, W.-J., Xia, H., Zhou, C.-G., 2014. Highly efficient removal of acid red 18 from aqueous solution by magnetically retrievable chitosan/carbon nanotube: batch study, isotherms, kinetics, and thermodynamics. J. Chem. Eng. Data 59 (1), 39–51.

Wang, Y., Li, L., Luo, C., Wang, X., Duan, H., 2016. Removal of Pb2+ from water environment using a novel magnetic chitosan/graphene oxide imprinted Pb2+. Int. J. Biol. Macromol. 86, 505–511.

Wang, F., Pan, Y., Cai, P., Guo, T., Xiao, H., 2017. Single and binary adsorption of heavy metal ions from aqueous solutions using sugarcane cellulose-based adsorbent. Bioresour. Technol. 241, 482–490.

Xing, B., Yuan, R., Zhang, C., Huang, G., Guo, H., Chen, Z., Chen, L., Yi, G., Zhang, Y., Yu, J., 2017. Facile synthesis of graphene nanosheets from humic acid for supercapacitors. Fuel Process. Technol. 165, 112–122.

Yan, H., Yang, H., Li, A., Cheng, R., 2016. pH-tunable surface charge of chitosan/graphene oxide composite adsorbent for efficient removal of multiple pollutants from water. Chem. Eng. J. 284, 1397–1405.

Zhao, C., Ma, L., You, J., Qu, F., Priestley, R.D., 2016. EDTA-and amine-functionalized graphene oxide as sorbents for Ni (II) removal. Desalination and Water Treatment 57 (19), 8942–8951.